Journal of Thermal Analysis and Calorimetry (2019) 136:401–409
https://doi.org/10.1007/s10973-018-7912-5

Second-order slip, cross-diffusion and chemical reaction effects on magneto-convection of Oldroyd-B liquid using Cattaneo–Christov heat flux with convective heating

K. Loganathan[1] · S. Sivasankaran[2] · M. Bhuvaneswari[2,3] · S. Rajan[1]

Received: 10 June 2018 / Accepted: 8 November 2018 / Published online: 22 November 2018

Abstract
The present article investigates the effect of second-order slip, chemical reaction and Soret and Dufour effects on MHD convective flow of an Oldroyd-B liquid toward a stretchy surface. Analysis of thermal relaxation time is made by using Cattaneo–Christov heat flux model. The effects of radiation and convective heating are also taken into account. The ordinary differential equations are retrieved by the help of suitable transformations of governing equations. The analytical solutions are observed by homotopy progress. The velocity, concentration and temperature field are analyzed for various pertinent parameters involved in the study. The graphical results of physical quantities of interest such as skin friction, local Nusselt number and local Sherwood number are presented. A comparative study with existing result indicates excellent agreement.

Keywords Second-order slip · Oldroyd-B fluid · Cattaneo–Christov heat flux · Convective heating · Soret and Dufour effects · Chemical reaction

List of symbols

A_1	Relaxation time
A_2	Retardation time
a	Stretching rate (s^{-1})
Bi	Biot number (–)
B_0	Constant magnetic field $(\mathrm{kg\,s^{-2}\,A^{-1}})$
c	Concentration $(\mathrm{kg\,m^{-3}})$
c_p	Specific heat $(\mathrm{J\,kg^{-1}\,K^{-1}})$
c_∞	Ambient concentration $(\mathrm{kg\,m^{-3}})$
c_w	Fluid wall concentration $(\mathrm{kg\,m^{-3}})$
C_f	Skin friction coefficient $(\frac{1+\alpha}{1+\beta}f''(0))$ (–)
Cr	Chemical reaction parameter (–)
D_m	Diffusion coefficient $(\mathrm{m^2\,s^{-1}})$
D_f	Dufour number (–)
$f(\eta)$	Velocity similarity function (–)
h_f	Convective heat transfer coefficient $(\mathrm{W\,m^{-1}\,K^{-1}})$
k	Thermal conductivity $(\mathrm{W\,m^{-1}\,K^{-1}})$
k_T	First-order chemical reaction parameter (–)
L	Auxiliary linear operator (–)
M	Hartmann number (–)
N	Nonlinear operator (–)
Nu_x	Nusselt number $(-(1+\frac{4}{3}R_d)\theta'(0))$ (–)
Pr	Prandtl number (–)
q_1	Heat flux $(\mathrm{W\,m^{-2}})$
R_d	Radiation constant (–)
Sc	Schmidt number (–)
Sr	Soret number (–)
Sh_x	Sherwood number $(-\phi'(0))$ (–)
T	Temperature (K)
T_∞	Ambient temperature (K)
T_w	Convective surface temperature (K)
u, v	Velocity components in (x, y) directions $(\mathrm{m\,s^{-1}})$
u_w	Velocity of the sheet $(\mathrm{m\,s^{-1}})$
x, y	Cartesian coordinates (m)

Greeks

α	Dimensionless relaxation time parameter (–)
β	Dimensionless retardation time parameter (–)

✉ S. Sivasankaran
sd.siva@yahoo.com

[1] Department of Mathematics, Erode Arts and Science College, Erode, Tamilnadu 638009, India

[2] Department of Mathematics, King Abdulaziz University, Jeddah 21589, Saudi Arabia

[3] Department of Mathematics, Kongunadu Polytechnic College, D. Gudalur, Tamilnadu, India

χ_m	Auxiliary parameter (–)
ϵ_1	Dimensionless first-order slip velocity parameter (–)
ϵ_2	Dimensionless second-order slip velocity parameter (–)
$\phi(\eta)$	Concentration similarity function (–)
γ	Dimensionless thermal relaxation time (–)
η	Similarity parameter (–)
λ_1	First-order slip velocity factor
λ_2	Second-order slip velocity factor
v	Kinematic viscosity $(\mathrm{m^2\,s^{-1}})$
$\theta(\eta)$	Temperature similarity function $(-)$
ρ	Density $(\mathrm{kg\,m^{-3}})$
σ	Electrical conductivity $(\mathrm{S\,m})$
ψ	Stream function $(\mathrm{m^2\,s^{-1}})$

Introduction

The flow of non-Newtonian fluids past a stretchy surface has attracted many scientists by interest of its engineering-related applications. These fluids did not satisfy the "Newton's law of viscosity", that is, these fluids change their flow behavior with respect to stress. Also, it cannot be interpreted the aspects of non-Newtonian fluids as a single constitutive relationship. Many investigators developed the different models of such fluids. Fourier heat statement yields parabolic energy equation which presents that the total system is immediately affected by the initial disturbance. To taken this issue, Cattaneo [1] altered Fourier's law of heat conduction in appearance of thermal relaxation. The hyperbolic-type energy equation exists in the presence of Cattaneo's statement. Christov [2] upgraded the analysis of Cattaneo [1] by involving thermal relaxation time with Oldroyd's upper-convected derivatives to attain the material invariant formulation. The Oldroyd-B liquid model is one of the non-Newtonian fluid models, which describes the retardation and relaxation effects. Hayat et al. [3] investigated about 2D MHD steady flow of an Oldroyd-B liquid with Cattaneo–Christov model. Li et al. [4] depicted the slip effects of MHD flow of viscoelastic fluid bounded by a vertical stretching sheet with Cattaneo–Christov heat flux model. Imtiaz et al. [5] provided the 2D third-grade liquid flow over a linear stretchy sheet with chemical reaction. Mixed convection flow of an Oldroyd-B liquid with cross-diffusion effects was analyzed by Ashraf et al. [6]. Effect of various non-Newtonian nanofluids over a cone was done by Reddy et al. [7]. Rashidi et al. [8] examined the second-order slip flow and heat transfer of a nanofluid toward a stretchy surface. Zhu et al. [9] studied the magneto-hydrodynamic flow and heat transfer with effects of the second-order velocity slip and temperature-jump boundary conditions. Vishnu Ganesh et al. [10] performed the magneto-hydrodynamic axisymmetric slip flow along a vertical stretching cylinder with convective heating.

In recent years, quite a large number of studies dealing with Dufour–Soret effects on mass and heat transfer of viscoelastic fluids have been appeared. Dufour and Soret effects combined with radiation and chemical reaction on Oldroyd-B liquid flow upon a stretchy surface with Cattaneo–Christov heat flux were analyzed by Loganathan et al. [11]. By using Lie group analysis, Bhuvaneswari et al. [12] explored the double-diffusive convective flow of an incompressible fluid past an inclined semi-infinite surface with first-order homogeneous chemical reaction. Siddiqa et al. [13] studied about Casson particulate suspension flow past a complex isothermal wavy surface with thermal radiation. Freidoonimehr et al. [14] obtained an analytical solution of heat and mass transfer for MHD three-dimensional flow toward a bidirectional stretching sheet with velocity slip conditions. The approximate analytical method of homotopy analysis is widely used in the flow and heat transfer problems to solve the highly nonlinear equations. This homotopy analysis method has been extensively used/studied in Refs. [15–19].

We attempt this study to explore the effects of second-order slip flow of an Oldroyd-B fluid toward a stretching surface in the appearance of radiation, convective heating, chemical reaction and cross-diffusion effects using Cattaneo–Christov heat flux model.

Flow analysis

Consider the two-dimensional MHD convective flow of an incompressible Oldroyd-B liquid over a linear stretchy sheet (Fig. 1). The velocity distributions (u, v) are taken in the (x, y)-directions, respectively. The velocity of sheet is assumed as $u_w = ax$, where $a > 0$ is the stretching rate. The two temperatures on and apart from the surface are expressed by T_w and T_∞ with $T_w > T_\infty$. Heat flux (q_1) in view of Cattaneo–Christov theory is expressed

$$q_1 + \lambda\left[\frac{\partial q_1}{\partial t} + V.\nabla q_1 - q_1.\nabla V + (\nabla.V)q_1\right] = -k_0\nabla T \tag{1}$$

in which λ is the thermal relaxation, V is the velocity and k is the fluid thermal conductivity. Equation (1) reduces to the classical Fourier's law when $\lambda = 0$. Finally, Eq. (1) for incompressible fluid case reduces to the following expression:

$$q_1 + \lambda\left(\frac{\partial q_1}{\partial t} + V.\nabla q_1 - q_1.\nabla V\right) = -k\nabla T \tag{2}$$

The magnetic field of strength B_0 is applied upright to the stretchy surface. The electric and induced magnetic fields

Fig. 1 Schematic diagram

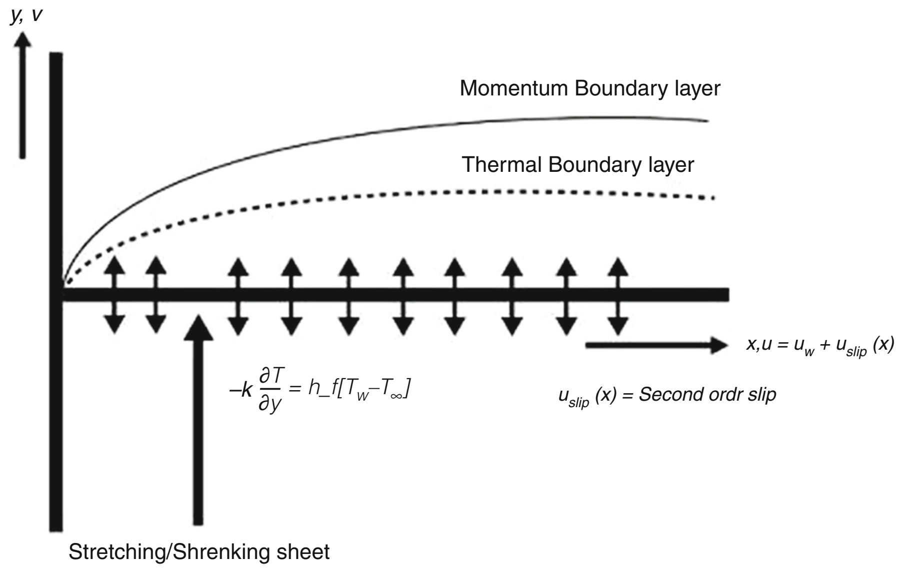

are neglected. The governing equations of the flow are taken as, see Hayat et al. [3]

$$\frac{\partial u}{\partial x}+\frac{\partial v}{\partial y}=0, \tag{3}$$

$$u\frac{\partial u}{\partial x}+v\frac{\partial u}{\partial y}+A_1\left(u^2\frac{\partial^2 u}{\partial x^2}+v^2\frac{\partial^2 u}{\partial y^2}+2uv\frac{\partial^2 u}{\partial x\partial y}\right)=\nu\frac{\partial^2 u}{\partial y^2}$$
$$-\nu A_2\left(u\frac{\partial^3 u}{\partial x\partial y^2}+v\frac{\partial^3 u}{\partial y^3}-\frac{\partial u}{\partial x}\frac{\partial^2 u}{\partial y^2}-\frac{\partial u}{\partial y}\frac{\partial^2 v}{\partial y^2}\right)$$
$$-\frac{\sigma B_0^2}{\rho}\left(u+A_1 v\frac{\partial u}{\partial y}\right), \tag{4}$$

$$u\frac{\partial T}{\partial x}+v\frac{\partial T}{\partial y}=\frac{k}{\rho c_{\mathrm{p}}}\frac{\partial^2 T}{\partial y^2}-\frac{1}{\rho c_{\mathrm{p}}}\frac{\partial q_{\mathrm{r}}}{\partial y}+\frac{D_{\mathrm{m}}k_{\mathrm{T}}}{c_{\mathrm{s}}c_{\mathrm{p}}}\frac{\partial^2 C}{\partial y^2} \tag{5}$$

$$u\frac{\partial C}{\partial x}+v\frac{\partial C}{\partial y}=D_{\mathrm{m}}\frac{\partial^2 C}{\partial y^2}-k_{\mathrm{m}}(C-C_\infty)+\frac{D_{\mathrm{m}}k_{\mathrm{T}}}{T_{\mathrm{m}}}\frac{\partial^2 T}{\partial y^2} \tag{6}$$

The corresponding boundary conditions are

$$u=u_{\mathrm{w}}+u_{\mathrm{slip}}=ax+\lambda_1\frac{\partial u}{\partial y}+\lambda_2\frac{\partial^2 u}{\partial y^2},\quad v=0,$$
$$-k\frac{\partial T}{\partial y}=h_{\mathrm{f}}(T_{\mathrm{w}}-T_\infty),\quad T=T_{\mathrm{w}}\quad C=C_{\mathrm{w}}\quad \text{at } y=0,$$
$$u\to 0,\quad v\to 0,\quad T\to T_\infty,\quad C\to C_\infty\quad \text{as } y\to\infty, \tag{7}$$

where ν, ρ, A_1 & A_2, c, c_{p}, σ, D_{m}, k_{T}, λ_1 & λ_2 are the kinematic viscosity, density, relaxation time and retardation time, concentration, specific heat, electrical conductivity, diffusion coefficient, first-order chemical reaction parameter and first- and second-order slip velocity factors, respectively. Using Cattaneo–Christov heat flux theory, we obtain the following energy equation

$$u\frac{\partial T}{\partial x}+v\frac{\partial T}{\partial y}+\lambda\left(u^2\frac{\partial^2 T}{\partial x^2}+v^2\frac{\partial^2 T}{\partial y^2}+\left(u\frac{\partial u}{\partial x}+v\frac{\partial u}{\partial y}\right)\frac{\partial T}{\partial x}\right.$$
$$\left.+2uv\frac{\partial T^2}{\partial x\partial y}+\left(u\frac{\partial v}{\partial x}+v\frac{\partial v}{\partial y}\right)\frac{\partial T}{\partial y}\right)$$
$$=\frac{k}{\rho c_{\mathrm{p}}}\frac{\partial^2 T}{\partial y^2}-\frac{1}{\rho c_{\mathrm{p}}}\frac{\partial q_{\mathrm{r}}}{\partial y}+\frac{D_{\mathrm{m}}k_{\mathrm{T}}}{c_{\mathrm{s}}c_{\mathrm{p}}}\frac{\partial^2 C}{\partial y^2} \tag{8}$$

The radiative heat flux is taken as

$$q_{\mathrm{r}}=-\frac{4\sigma_0}{3k^*}\frac{\partial T^4}{\partial y} \tag{9}$$

Consider the following similarity transformations

$$\psi=\sqrt{a\nu}xf(\eta),\quad u=\frac{\partial\psi}{\partial y},\quad v=-\frac{\partial\psi}{\partial x},\quad \eta=\sqrt{\frac{a}{\nu}}y$$
$$v=-\sqrt{a\nu}f(\eta),\quad u=axf'(\eta),\quad \theta(\eta)=\frac{T-T_\infty}{T_{\mathrm{w}}-T_\infty},$$
$$\phi(\eta)=\frac{C-C_\infty}{C_{\mathrm{w}}-C_\infty} \tag{10}$$

Substituting Eq. (10) in Eqs. (4), (6) and (8), we have

$$f'''+\beta\left(f''^2-ff^{\mathrm{iv}}\right)+\alpha\left(2ff'f''-f^2f'''\right)$$
$$+ff''-f'^2-M(f'-\alpha ff'')=0 \tag{11}$$

$$\frac{1}{Pr}\left(1+\frac{4}{3}R_{\mathrm{d}}\right)\theta''+f\theta'-\gamma\left(f^2\theta''+ff'\theta'\right)+D_{\mathrm{f}}\phi''=0 \tag{12}$$

$$\frac{1}{Sc}\phi''+f\phi'-Cr\phi+Sr\theta''=0 \tag{13}$$

with boundary conditions

$$
\begin{aligned}
&f(0)=0,\ f'(0)=1+\epsilon_1 f''(0)+\epsilon_2 f'''(0),\\
&\quad \theta'(0)=-Bi(1-\theta(0)),\quad \phi(0)=1\\
&\quad f'(\infty)=0,\quad \theta(\infty)=0,\quad \phi(\infty)=0,
\end{aligned}
\tag{14}
$$

Here we declare the dimensionless variables as follows: $\epsilon_1=\lambda_1\sqrt{a/v}$ & $\epsilon_2=\lambda_2\frac{a}{v}$ are the first- and second-order slip velocity constants, $\frac{h_f}{k}\sqrt{v/a}$ is the Biot number, $\alpha=A_1 a$ and $\beta=A_2 a$ are the dimensionless relaxation and retardation time constants, respectively, $M=\frac{\sigma B_0^2}{\rho a}$ the Hartmann number, $Pr=\frac{\rho v C_p}{k}$ the Prandtl number, $R_d=\frac{4\sigma^* T_\infty^3}{kk^*}$ the thermal radiation parameter, $\gamma=\lambda a$, the non-dimensional thermal relaxation time, $D_f=\frac{D_m k_T}{v c_s c_p}\frac{c_w-c_\infty}{T_w-T_\infty}$, the Dufour number, $Cr=\frac{k_m}{a}$ the chemical reaction constant, $Sc=\frac{v}{D_m}$ the Schmidt number, $Sr=\frac{D_m k_T}{v T_m}\frac{T_w-T_\infty}{c_w-c_\infty}$ the Soret number.

The dimensionless forms of local skin friction ($Re^{\frac{1}{2}}Cf_x$), heat ($Re^{-\frac{1}{2}}Nu_x$) and mass ($Re^{-\frac{1}{2}}Sh_x$) transfer rates are represented below

$$
\begin{aligned}
Re^{\frac{1}{2}}Cf_x &= \frac{1+\alpha}{1+\beta}f''(0)\\
Re^{-\frac{1}{2}}Nu_x &= -\left(1+\frac{4}{3}R_d\right)\theta'(0)\\
Re^{-\frac{1}{2}}Sh_x &= -\phi'(0)
\end{aligned}
$$

Solution methodology

We incorporated the homotopy analysis method in order to get the convergent solution of the system of equations. The initial approximations and complementary linear operators can be put in the form

$$
\begin{aligned}
&f_0=\eta e^{-\eta}+\frac{3\epsilon_2-2\epsilon_1}{\epsilon_2-1-\epsilon_1}*e^{-\eta}-\frac{3\epsilon_2-2\epsilon_1}{\epsilon_2-1-\epsilon_1},\\
&\theta_0=\frac{Bi*e^{-\eta}}{1+Bi},\qquad \phi_0=e^{-\eta}.\ L_f=f'''-f',\\
&\quad L_\theta=\theta''-\theta,\qquad L_\phi=\phi''-\phi
\end{aligned}
$$

which satisfies the property

$$
\begin{aligned}
&L_f[D_1+D_2e^{\eta}+D_3e^{-\eta}]=0,\quad L_\theta[D_4e^{\eta}+D_5e^{-\eta}]=0,\\
&L_\phi[D_6e^{\eta}+D_7e^{-\eta}]=0,
\end{aligned}
$$

where $D_k(k=1-7)$ are constants. The zeroth-order deformation equation is constructed as

$$
(1-p)L_f\left[\widehat{f}(\eta;p)-f_0(\eta)\right]=pH_f h_f N_f\left[\widehat{f}(\eta;p)\right]
\tag{15}
$$

$$
\begin{aligned}
&(1-p)L_\theta\left[\widehat{\theta}(\eta;p)-\theta_0(\eta)\right]\\
&\quad =pH_\theta h_\theta N_\theta\left[\widehat{\theta}(\eta;p),\ \widehat{f}(\eta;p),\widehat{\phi}(\eta;p)\right]
\end{aligned}
\tag{16}
$$

$$
\begin{aligned}
&(1-p)L_\phi\left[\widehat{\phi}(\eta;p)-\phi_0(\eta)\right]\\
&\quad =pH_\phi h_\phi N_\phi\left[\widehat{\phi}(\eta;p),\ \widehat{f}(\eta;p),\ \widehat{\theta}(\eta;p)\right].
\end{aligned}
\tag{17}
$$

where the system of nonlinear operators in HAM for the present problem is

$$
\begin{aligned}
N_f\left[\widehat{f}(\eta;p)\right] &= \frac{\partial^3\widehat{f}(\eta;p)}{\partial\eta^3}-\left(\frac{\partial\widehat{f}(\eta;p)}{\partial\eta}\right)^2+\widehat{f}(\eta;p)\frac{\partial^2\widehat{f}(\eta;p)}{\partial\eta^2}\\
&+\alpha\left(2\widehat{f}(\eta;p)\frac{\partial\widehat{f}(\eta;p)}{\partial\eta}\frac{\partial^2\widehat{f}(\eta;p)}{\partial\eta^2}-\left(\widehat{f}(\eta;p)\right)^2\frac{\partial^3\widehat{f}(\eta;p)}{\partial\eta^3}\right)\\
&+\beta\left(\left(\frac{\partial^2\widehat{f}(\eta;p)}{\partial\eta^2}\right)^2-\widehat{f}(\eta;p)\frac{\partial^4\widehat{f}(\eta;p)}{\partial\eta^4}\right)\\
&-M\left(\frac{\partial\widehat{f}(\eta;p)}{\partial\eta}-\alpha\widehat{f}(\eta;p)\frac{\partial^2\widehat{f}(\eta;p)}{\partial\eta^2}\right)
\end{aligned}
\tag{18}
$$

$$
\begin{aligned}
&N_\theta\left[\widehat{f}(\eta;p),\ \widehat{\theta}(\eta;p),\ \widehat{\phi}(\eta;p)\right]\\
&=\left(1+\frac{4}{3}R_d\right)\frac{\partial^2\widehat{\theta}(\eta;p)}{\partial\eta^2}+Pr\widehat{f}(\eta;p)\frac{\partial\widehat{\theta}(\eta;p)}{\partial\eta}\\
&\quad -Pr\gamma\left(\widehat{f}(\eta;p)\frac{\partial\widehat{f}(\eta;p)}{\partial\eta}\frac{\partial\widehat{\theta}(\eta;p)}{\partial\eta}+\left(\widehat{f}(\eta;p)\right)^2\frac{\partial^2\widehat{\theta}(\eta;p)}{\partial\eta^2}\right)\\
&\quad +PrD_f\left(\frac{\partial^2\widehat{\phi}(\eta;p)}{\partial\eta^2}\right)
\end{aligned}
\tag{19}
$$

$$
\begin{aligned}
&N_\phi\left[\widehat{f}(\eta;p),\ \widehat{\theta}(\eta;p),\widehat{\phi}(\eta;p)\right]\\
&=\frac{\partial^2\widehat{\phi}(\eta;p)}{\partial\eta^2}+Sc\widehat{f}(\eta;p)\frac{\partial\widehat{\phi}(\eta;p)}{\partial\eta}\\
&\quad -Sc\ Cr\ \widehat{\phi}(\eta;p)+ScSr\left(\frac{\partial^2\widehat{\theta}(\eta;p)}{\partial\eta^2}\right)
\end{aligned}
\tag{20}
$$

The boundary conditions are

$$
\begin{aligned}
&\widehat{f}(0;p)=0,\widehat{f}'(0;p)=1+\epsilon_1\widehat{f}''(0;p)\\
&\qquad +\epsilon_2\widehat{f}'''(0;p),\widehat{f}'(\infty;p)=0,\\
&\widehat{\theta}'(0;p)=-Bi\left(1-\widehat{\theta}(0;p)\right),\widehat{\theta}(\infty;p)=0,\\
&\widehat{\phi}(0;p)=(1;p),\widehat{\phi}(\infty;p)=0.
\end{aligned}
\tag{21}
$$

The mth-order deformation equations are

$$
L_f(f_m(\eta)-\chi_m f_{m-1}(\eta))=h_f R_m^f(\eta)
\tag{22}
$$

$$
L_\theta(\theta_m(\eta)-\chi_m\theta_{m-1}(\eta))=h_\theta R_m^\theta(\eta)
\tag{23}
$$

$$L_\phi(\phi_m(\eta) - \chi_m\phi_{m-1}(\eta)) = h_\phi R_m^\phi(\eta) \tag{24}$$

subject to the boundary conditions

$$\begin{aligned} &f_m(0) = 0,\ f_m'(0) - \epsilon_1 f_m''(0) - \epsilon_2 f_m'''(0) = 0 \text{ and} \\ &f_m'(\eta) \to 0 \text{ when } \eta \to \infty \\ &\theta_m'(0) - Bi\theta_m(0) = 0 \text{ and} \\ &\theta_m(\eta) \to 0 \text{ when } \eta \to \infty \\ &\phi_m'(0) = 0 \text{ and } \phi_m(\eta) \to 0 \text{ when } \eta \to \infty \end{aligned} \tag{25}$$

$$\begin{aligned} R_m^f(\eta) = &f_{m-1}''' + \Sigma_{k=0}^{m-1}\left[f_{m-1-k}f_k'' - f_{m-1-k}'f_k'\right] \\ &+ \alpha\Sigma_{l=0}^{m-1}f_{m-1-l}\left(2\Sigma_{j=0}^{l}f_{l-j}'f_j'' + \Sigma_{j=0}^{l}f_{l-j}f_j'''\right) \\ &+ \beta\Sigma_{k=0}^{m-1}\left[f_{m-1-k}''f_k'' - f_{m-1-k}f_k^{iv}\right] \\ &- M\left(f_{m-1} - \alpha\Sigma_{k=0}^{m-1}f_{m-1-k}f_k''\right) \end{aligned} \tag{26}$$

$$\begin{aligned} R_m^\theta(\eta) = &\left(1 + \frac{4}{3}R_d\right)\theta_{m-1}'' + Pr\Sigma_{l=0}^{m-1}\left[\theta_{m-1-l}'f_l\right] \\ &- Pr\gamma\left(f_{m-1-l}\Sigma_{j=0}^{l}f_{l-j}'\theta_j' + f_{m-1-l}\theta_l''\right) \\ &+ PrD_f\Sigma_{k=0}^{m-1}\phi_{m-1}'' \end{aligned} \tag{27}$$

$$\begin{aligned} R_m^\phi(\eta) = &\frac{1}{Sc}\phi_{m-1}'' + \Sigma_{k=0}^{m-1}f_{m-1-k}\phi_k' - Cr\phi_{m-1} \\ &+ Sr\Sigma_{k=0}^{m-1}\theta_{m-1}'' \end{aligned} \tag{28}$$

where $\chi_m = \begin{cases} 0, & m \le 1, \\ 1, & m \ge 1. \end{cases}$

After solving mth -order HAM equations, we get the followings

$$\begin{aligned} f_m(\eta) &= f_m^*(\eta) + D_1 + D_2e^{\eta} + D_3e^{-\eta} \\ \theta_m(\eta) &= \theta_m^*(\eta) + D_4e^{\eta} + D_5e^{-\eta} \\ \phi_m(\eta) &= \phi_m^*(\eta) + D_6e^{\eta} + D_7e^{-\eta} \end{aligned}$$

The $f_m^*(\eta)$, $\theta_m^*(\eta)$ and $\phi_m^*(\eta)$ are the special solutions of the equations. The complementary constants h_f, h_θ and h_ϕ perform a key role and the fields are drawn at fifteenth order of approximation to accomplish the valid range of constants (see Fig. 2). The acceptable values of h_f, h_θ and h_ϕ are $-1.7 \le h_f \le -0.6, -1.2 \le h_\theta \le -0.6, -1.2 \le h_\phi \le -0.3$, respectively. Table 1 shows the order of approximation for HAM. Table 2 depicts $f''(0)$ in the absence of MHD and retardation time parameter. It is observed that all obtained values of $f''(0)$ are in an excellent agreement with the values found in Sadghey et al. [20], Mukhopadhyay [21] and Abbasi et al. [22]. A comparison of $-f''(0)$ and $-\theta'(0)$ has been made between the results of the HAM solution and the results in Ref. [3] in Table 3.

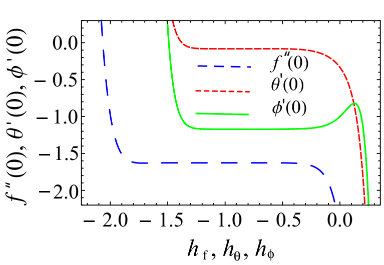

Fig. 2 h-curves for h_f, h_θ, h_ϕ

Table 1 Order of approximations

Order	$-f''(0)$	$-\theta'(0)$	$-\phi'(0)$
1	2.0422	0.2363	1.0687
5	1.6491	0.1046	1.1607
10	1.6277	0.0818	1.1707
15	1.6274	0.0817	1.1717
20	1.6274	0.0821	1.1715
25	1.6274	0.0820	1.1715
30	1.6274	0.0820	1.1715
40	1.6274	0.0820	1.1715
50	1.6274	0.0820	1.1715

Results and discussion

The numerical values of velocity, concentration and temperature distributions are computed through various combination of parameters involved in this study with the fixed values of $\epsilon_1 = 0.2$, $\epsilon_2 = 0.3$, $M = 0.5$, $\alpha = 0.1$, $\beta = 0.1$, $\gamma = 0.5$, $R_d = 0.3$, $Pr = 1.0$, $D_f = 0.5$, $Sc = 0.9$, $Bi = 0.5$, $Cr = 1.0$, $Sr = 0.3$.

Effect on velocity

It is surveyed from Fig. 3 that the velocity diminishes while increasing the values of relaxation time constant. This is due to increasing the stretching rate of the sheet which reduces the flow speed. Figure 4 demonstrates that the velocity decreases near boundary and rises after some distance when raising the values of retardation time constant. Increasing stretching rate affects retardation time parameter which provides this peculiar result. The velocity profile slowly diminishes on increasing the values of first-order slip constant, which is plotted in Fig. 5. Figure 6 indicates that the velocity enhances when the second-order slip constant rises. Here viscosity of the fluid reduces on increasing ϵ_2. When comparing Figs. 5 and 6, the effect of first-order slip constant on velocity is more pronounced than the second-order slip constant.

Table 2 Comparison with $f''(0)$ obtained by Sadghey et al. [20], Mukhopadhyay [21] and Abbasi et al. [22] in the limiting case for different α by fixing $\beta = M = 0$

α	Sadghey et al. [20]	Mukhopadhyay. [21]	Abbasi et al. [22]	Present
0.0	1.000	0.9999963	1.00000	1.00000
0.2	1.0549	1.051949	1.05189	1.05189
0.4	1.10084	1.101851	1.10190	1.10190
0.6	1.0015016	1.150162	1.15014	1.15014
0.8	1.19872	1.196693	1.19671	1.19671

Table 3 Comparison with $-f''(0)$ and $-\theta'(0)$ obtained by Hayat et al. [3], when $\epsilon_1 = \epsilon_2 = R_d = D_f = Bi = 0$

Mode	$-f''(0)$		$-\theta'(0)$	
Order	Hayat et al. [3]	Present	Hayat et al. [3]	Present
1	1.1833	1.1833	0.61111	0.61111
5	1.1439	1.1439	0.54844	0.54844
12	1.1435	1.1435	0.54642	0.54642
20	1.1435	1.1435	0.54642	0.54642
30	1.1435	1.1435	0.54642	0.54642

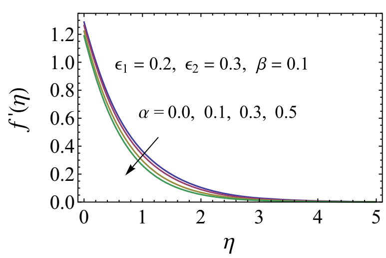

Fig. 3 Velocity variations for different ranges of relaxation time parameter (α)

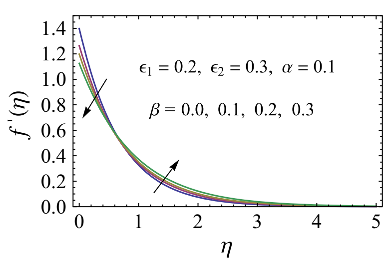

Fig. 4 Velocity variations for different ranges of retardation time parameter (β)

Effect on temperature

The influence of thermal relaxation time for heat flux γ on the temperature profile is analyzed in Fig. 7. It can be archived that the temperature in Cattaneo–Christov heat flux model is less than the Fourier's model. Figure 8 displays the impact of radiation parameter on temperature. By raising the values of radiation parameter, the thermal boundary layer thickness develops. Raising the radiation

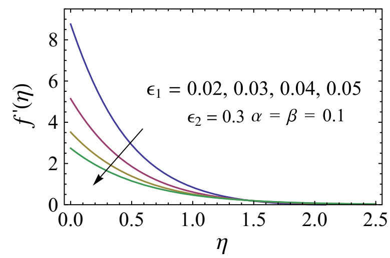

Fig. 5 Velocity variations for different ranges of first-order velocity slip parameter (ϵ_1)

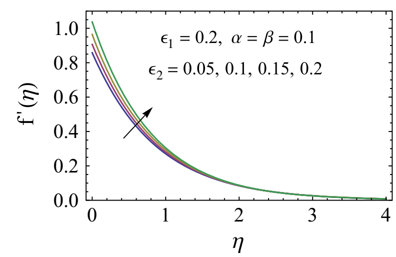

Fig. 6 Velocity variations for different ranges of second-order velocity slip parameter (ϵ_2)

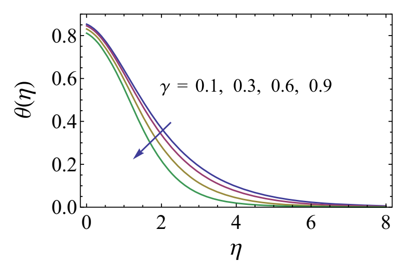

Fig. 7 Temperature variations for different ranges of thermal relaxation time parameter (γ)

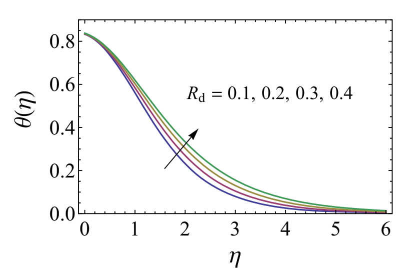

Fig. 8 Temperature variations for different ranges of radiation parameter (R_d)

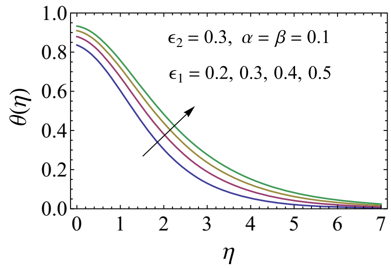

Fig. 9 Temperature variations for different ranges of first-order velocity slip parameter (ϵ_1)

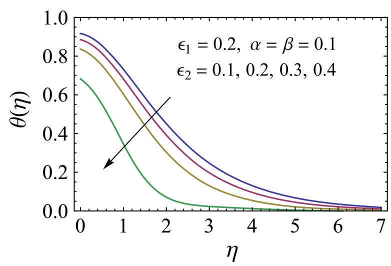

Fig. 10 Temperature variations for different ranges of second-order velocity slip parameter (ϵ_2)

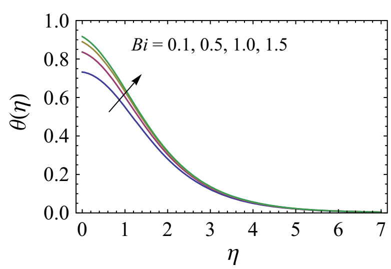

Fig. 11 Temperature variations for different ranges of Biot number (Bi)

parameter enhances the thermal conductivity of the medium and it results in the growth of thermal boundary layer. It is seen from Figs. 9 and 10 that first- and second-order slip constants showed the opposing tendency on temperature profile. Figure 11 shows the effect of Biot number on temperature profile. It shows that temperature is growing function of Bi near the surface because the Biot number affects much the temperature near the surface. Rising values of Bi are due to higher heat transfer resistance inside a body as compared to surface. The impact of Dufour number on temperature is sketched in Fig. 12. It is concluded that the thermal boundary layer thickness boosted up on raising the values of Dufour number.

Effect on concentration

Figure 13 demonstrates the effect of chemical reaction on concentration profile. It shows that concentration reduces on higher values of chemical reaction parameter. It is inspected from Fig. 14 that a rise in Soret number initially gives less effect on concentration, while the tremendous trend occurs when $\eta > 1$. That is, concentration rises with Soret number after $\eta > 1$.

Local skin friction, Nusselt number and Sherwood number

The effects of ϵ_1, ϵ_2 with α on skin friction are investigated through Figs. 15 and 16. Apparently, first- and second-order slip constants with relaxation time have opposite effects on skin friction. Figure 17 presents the effects of both the first-order slip constant ϵ_1 and the magnetic field constant M on the local Nusselt number. The graph represented that the heat transfer rate decreases when ϵ_1 increases. Figure 18 depicts the influence of both the second-order slip constant ϵ_2 and the magnetic field constant M on the local Nusselt number. From the figure, we can observe that the heat transfer rate on the surface enhances when the second-order slip constant ϵ_2 increases. Figures 19 and 20 explore the variation of the local Sherwood number. It is clear that the local mass transfer rate diminishes with the growth of α and Cr, and it decreases on raising the value of M and Cr. Comparing these figures, it is concluded that the first- and second-order slip constants provide opposite tendency on physical quantities.

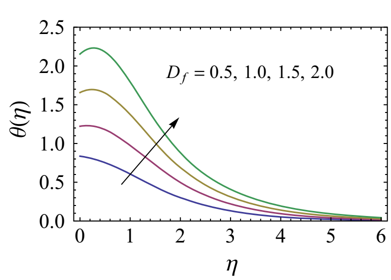

Fig. 12 Temperature variations for different ranges of Dufour number (D_f)

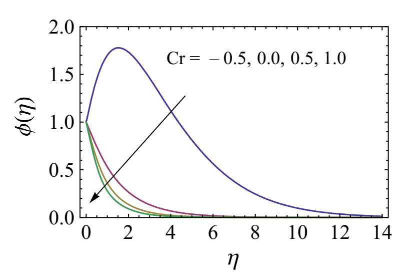

Fig. 13 Concentration variations for different range of Chemical reaction parameter (Cr)

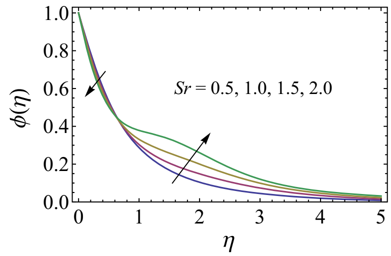

Fig. 14 Concentration variations for different range of Soret number (Sr)

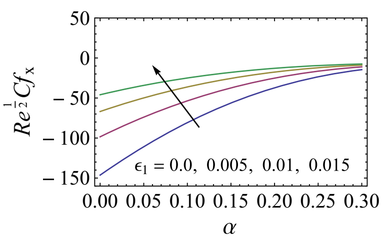

Fig. 15 Local skin friction for various values of ϵ_1 versus α

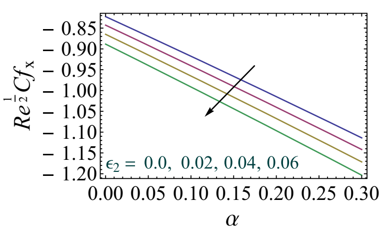

Fig. 16 Local skin friction for various values of ϵ_2 versus α

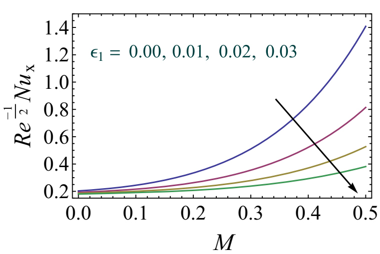

Fig. 17 Local Nusselt number for various values of ϵ_1 versus M

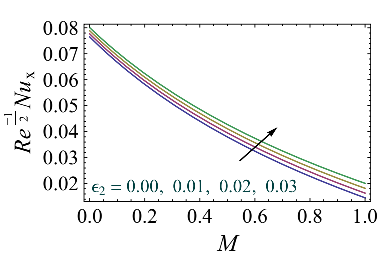

Fig. 18 Local Nusselt number for various values of ϵ_2 versus M

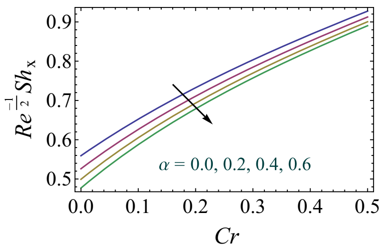

Fig. 19 Local Sherwood number for various values of α versus Cr

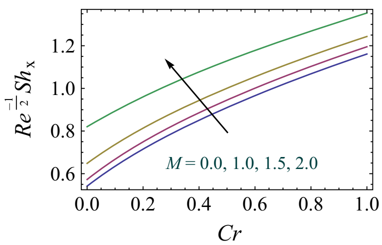

Fig. 20 Local Sherwood number for various values of M versus Cr

Conclusions

The present study reports the second-order slip and chemical reaction on steady two-dimensional flow of an incompressible Oldroyd-B liquid over a stretching sheet with convective heating. The following observations are found.

1. The skin friction enhances with first-order velocity slip, and it diminishes with second-order velocity slip.
2. The chemical reaction boosted up the mass transfer rate. Similar behavior on mass transfer rate with magnetic field is observed.
3. The first-order velocity slip provides much effect on heat transfer rate comparing second-order velocity slip while increasing Hartmann number.

References

1. Cattaneo C. Calore Sulla Conduzione. Del Atti Sem Mat Fis Univ Modena. 1948;3:83–101.
2. Christov CI. On frame indifferent formulation of the Maxwell–Cattaneo model of finite speed heat conduction. Mech Res Commun. 2009;36:481–6.
3. Hayat T, Imtiaz M, Alsaedi A, Almezal S. On Cattaneo–Christov heat flux in MHD flow of Oldroyd-B fluid with homogeneous–heterogeneous reactions. J Magn Mater. 2016;401(1):296–303.
4. Li J, Zheng L, Liu L. MHD viscoelastic flow and heat transfer over a vertical stretching sheet with Cattaneo–Christov heat flux effects. J Mol Liq. 2016;221:19–25.

5. Imtiaz M, Alsaedi A, Shaq A, Hayat T. Impact of chemical reaction on third grade fluid flow with Cattaneo–Christov heat flux. J Mol Liq. 2017;229:501–7.
6. Ashraf B, Hayat T, Alsaedi A, Shehzad SA. Soret and Dufour effects on the mixed convection flow of an Oldroyd-B fluid with convective boundary conditions. Results Phys. 2016;6:917–24.
7. Reddy GK, Yarrakula K, Raju CS. Mixed convection analysis of variable heat source/sink on MHD Maxwell, Jeffrey and Oldroyd-B nanofluids over a cone with convective conditions using Buongiorno's model. J Therm Anal Calorim. 2018;132(3): 1995–2002.
8. Rashidi MM, Abdul Hakeem AK, Vishnu Ganesh N, Ganga B, Sheikholeslami M, Momoniat E. Analytical and numerical studies on heat transfer of a nanofluid over a stretching/shrinking sheet with second-order slip flow model. Int J Mech Mater Eng. 2016;11:1.
9. Zhu J, Zheng L, Zheng L, Zhang X. Second-order slip MHD flow and heat transfer of nanofluids with thermal radiation and chemical reaction. Appl Math Mech. 2015;36(9):1131–46.
10. Vishnu Ganesh N, Ganga B, Abdul Hakeem AK, Saranya SC, Kalaivanan R. Hydromagnetic axisymmetric slip flow along a vertical stretching cylinder with convective boundary condition. St Petersb Polytech Univ J Phys Math. 2016;2:273–80.
11. Loganathan K, Sivasankaran S, Bhuvaneswari M, Rajan S. Dufour and Soret effects on MHD convection of Oldroyd-B liquid over stretching surface with chemical reaction and radiation using Cattaneo–Christov heat flux. In: IOP: Materials science and engineering. vol 390; 2018. p. 012077.
12. Bhuvaneswari M, Sivasankaran S, Kim YJ. Lie group analysis of radiation natural convection flow over an inclined surface in a porous medium with internal heat generation. J Porous Media. 2012;15(12):1155–64.
13. Siddiqa S, Begum N, Hossain MA, Shoaib M, Reddy Gorla RS. Radiative heat transfer analysis of non-Newtonian dusty Casson fluid flow along a complex wavy surface. Numer Heat Transf. 2018;73(4):209–21.
14. Freidoonimehr N, Rahimi AB. Brownian motion effect on heat transfer of a three-dimensional nanofluid flow over a stretched sheet with velocity slip. J Therm Anal Calorim. 2018. https://doi.org/10.1007/s10973-018-7060-y.
15. Golafshan B, Rahimi AB. Effects of radiation on mixed convection stagnation-point flow of MHD third-grade nanofluid over a vertical stretching sheet. J Therm Anal Calorim. 2018. https://doi.org/10.1007/s10973-018-7075-4.
16. Ghasemi SE, Hatami M, Sarokolaie AK, Ganji D. Study on blood flow containing nanoparticles through porous arteries in presence of magnetic field using analytical methods. Physica E. 2015;70:14656.
17. Liao S, Tan Y. A general approach to obtain series solutions of nonlinear differential. Stud Appl Math. 2007;119(4):297–354.
18. Kuznetsov A, Nield D. Natural convective boundary-layer flow of a nanofluid past a vertical plate: a revised model. Int J Therm Sci. 2014;77:1269.
19. Eswaramoorthi S, Bhuvaneswari M, Sivasankaran S, Rajan S. Soret and Dufour effects on viscoelastic boundary layer flow over a stretching surface with convective boundary condition with radiation and chemical reaction. Sci Iran B. 2016;23(6):2575–86.
20. Sadeghy K, Hajibeygi H, Taghavi SM. Stagnation-point flow of upper-convected Maxwell fluids. Int J Non-linear Mech. 2006;41:1242.
21. Mukhopadhyay S. Heat transfer analysis of the unsteady flow of a Maxwell fluid over a stretching surface in the presence of a heat source/sink. Chin Phys Lett. 2012;29:054703.
22. Abbasi FM, Mustafa M, Shehzad SA, Alhuthali MS, Hayat T. Analytical study of Cattaneo–Christov heat flux model for a boundary layer flow of Oldroyd-B fluid. Chin Phys B. 2016;25(1):014701.